Joint analysis of ISM and TES spectra: The utility of multiple wavelength regimes for Martian surface studies

John F. Mustard and Christopher D. Cooper
Department of Geological Sciences, Brown University, Providence, Rhode Island, USA

Received 26 August 2004; revised 4 March 2005; accepted 8 April 2005; published 28 May 2005.

[1] A number of spectroscopic instruments with high resolution and complementary wavelength ranges, including TES, THEMIS, OMEGA, and CRISM, will give an unprecedented wealth of information about the surface of Mars. In order to maximize the utility of these data sets, they need to be joined to provide pan-spectral coverage of the surface of Mars that will give information on different types of absorption processes in surface materials. We have performed a test of this approach using ISM and TES data to provide near-infrared and thermal infrared coverage of the selected regions observed by both instruments. Gridding and registering the two data sets to a common reference allows investigations of regional and global properties of the surface. Here we investigate the variability in the spectral properties of low-albedo regions, particularly Type I (basaltic) and Type II regions, and relate these variations to probably mineralogic composition. ISM and TES data agree on the presence of pyroxenes in Type I regions but may indicate a lack of pyroxene in the Type II material, although this is inconclusive. Type I regions in general appear to be uniform in composition, and surface variations are primarily controlled by mixing with dust. Temporal variations in surface reflectance make analysis of the differences in spectral properties between eastern and western Syrtis Major difficult but indicate that slope differences may not be due to intimate cementing of dark and light materials but rather due to penetrative oxidation of the surfaces of basaltic materials. These results demonstrate that the complementary strengths of multiple wavelength regimes allow greater understanding of surface composition and processes.

Citation: Mustard, J. F., and C. D. Cooper (2005), Joint analysis of ISM and TES spectra: The utility of multiple wavelength regimes for Martian surface studies, *J. Geophys. Res.*, *110*, E05012, doi:10.1029/2004JE002355.

1. Introduction

[2] In the next three years two important visible to near-infrared (vis-NIR) imaging spectrometers will arrive at Mars. The Compact Reconnaissance Imaging Spectrometer for Mars (CRISM) [*Murchie et al.*, 2003] instrument on the Mars Reconnaissance Orbiter spacecraft (expected arrival early 2006) and the Observatoire pour la Minéralogie, l'Eau, la Glace et l'Activité (OMEGA) on the Mars Express spacecraft [*Bibring et al.*, 2004] is returning data and creating the first global coverage of Mars in the vis-NIR at high spatial and spectral resolutions. The data from these instruments will complement the TES and THEMIS thermal infrared (TIR) data sets that have been and are being gathered from current missions at Mars. Together, data from these instruments will provide an unprecedented amount of information about the surface composition of Mars. An important key in maximizing the utility of these multiple data sets will be to analyze them simultaneously. Joining the data and performing analyses on the greater data set has the potential to yield insights into surface compositions and processes that may be unattainable by simply comparing results from independent analyses of the individual data sets.

[3] Joint analysis of spectral data sets has been done on a limited basis previously. *Mustard and Bell* [1994] compared telescopic visible spectra with Imaging Spectrometer for Mars (ISM) NIR image cubes. They found good agreement between the data sets and attributed most differences to the much better spatial resolution of ISM. *Erard and Calvin* [1997] combined Mariner 6 and 7 IRS measurements with ISM and telescopic data to extend the spectral range from 0.4 to 5.7 μm. They too found strong consistency across a twenty year span of measurements in the limited regions of spectral overlap. They found that the different spectral regions were dominated by different soil components, with palagonitic analog materials matching the longer wavelength portions of the joint spectra while hematite dominated the shorter wavelength regions. Both *Mustard and Bell* [1994] and *Erard and Calvin* [1997] found clear evidence for pyroxenes as well, consistent with the analysis of ISM data apart from other spectral data sets. Many laboratory studies have been performed over multiple wavelength regimes including investigations on the spectral properties of Martian meteorites

0148-0227/05/2004JE002355$09.00

Table 1. Comparison of Spectral Observations of Mars[a]

Instrument	Year	Wavelength Range	Spectral Sampling	Number of Channels	Pixel Size	Spatial Coverage
ISM	1989	0.77–3.14 μm	0.028–0.044 μm	64	22 km	9 regions @ 2600 × 550 km
OMEGA	2004–2006	0.5–5.2 μm	0.007–0.020 μm	352	0.3 km	2–5%
					4 km	global
CRISM	2006–2008	0.40–4.05 μm	0.007 μm	560	18 m	4%
				59	0.1–0.2 km	global
TES	1998–2004	6–50 μm	10 cm^{-1}	137	3 × 6 km	global
		(1650–200 cm^{-1})	5 cm^{-1}	286		
THEMIS	2002–2004	0.425–0.86 μm	0.1 μm	5	19 m	17%
		6.78–14.88 μm	1 μm	9	100 m	global

[a]Note: Percentages in spatial coverage refer to portion of Mars covered. Some instruments have multiple spatial resolution modes, while THEMIS has two instruments (VIS and TIR).

[*Bishop et al.*, 1998a, 1998b]. The analysis of ALH84001 showed that the measurements of both major minerals [*Bishop et al.*, 1998b] and minor constituents [*Bishop et al.*, 1998a] were enhanced using multiple wavelength regions including vis-NIR and TIR.

[4] Unlike these earlier cases of merging telescopic, ISM, and IRS data, this study expands the spectral data fusion across a wider wavelength range by combining ISM and TES data sets. This approach provides a key advantage from which previous studies of single data sets or the merged telescopic-ISM data have not benefited, namely the fact that ISM and TES together cover portions of the electromagnetic spectrum with fundamentally different absorption mechanisms. The vis-NIR region is dominated by charge transfer and electronic transition absorptions that are due to iron and other transition metals in geologic materials and by overtones of longer wavelength absorptions from key anions of rock-forming minerals [*Burns*, 1993; *Gaffey et al.*, 1993]. The TIR in contrast has fundamental absorptions that arise from vibrations of covalent bonds in crystal lattices. These absorptions arise in a wider range of geologic materials and include important information about the silicon-oxygen bonds in silicates that is unavailable in the vis-NIR [e.g., *Salisbury et al.*, 1991].

[5] Spectral data fusion across these wavelength regions will be especially important in the future as OMEGA and CRISM return terabytes of high-resolution data that can be combined with existing high-quality TES and THEMIS data (see Table 1 for comparisons). Here we assess the utility of joint analysis applied to the ISM and TES data for Mars research. With just the limited spatial coverage of the ISM data in the NIR portion of the spectrum combined with the TES TIR data, this study is able to address several important science questions relating to variations in the spectral properties of dark regions, variations across Syrtis Major, and relationships to mafic mineralogy. These results hold promise that global coverage at higher resolutions extended across many wavelength regimes can reveal even more about the surface properties of Mars.

2. Background

[6] Remotely sensed spectroscopic observations of Mars include data acquired by the thermal infrared spectrometers on the Mariner 9 [*Hanel et al.*, 1972; *Conrath et al.*, 1973] and Mars Global Surveyor orbiters [e.g., *Christensen et al.*, 1998, 2001; *Bandfield et al.*, 2000b]; multispectral imagers on the Vikings (visible) [e.g., *Soderblom et al.*, 1978; *Arvidson et al.*, 1982] and Mars Odyssey (vis-NIR and thermal IR) [*Christensen et al.*, 2003] spacecraft; Earth-based, telescope-mounted spectrometers [e.g., *Singer*, 1982, 1985; *Clark et al.*, 1990; *Pollack et al.*, 1990; *Blaney and McCord*, 1995]; the Hubble Space Telescope [*Bell et al.*, 1997]; and the near infrared spectrometer on the Phobos II spacecraft [e.g., *Bibring et al.*, 1990; *Erard et al.*, 1991]. As of early 2005, the OMEGA visible to near-IR imaging spectrometer [*Bibring et al.*, 2005] on board the Mars Express spacecraft has acquired near global coverage of Mars while the CRISM instrument [*Murchie et al.*, 2003] will arrive in 2006.

[7] These observations have provided a picture of the major types of surface materials and their distribution. In particular, the Viking color data, ISM, and TES have covered large areas on the regional to global scale and have created a framework to analyze the Martian surface. Viking color data combined with thermal inertia studies divided the surface up into three primary types shown in Figure 1: dark gray, dark red, and bright red regions [*Soderblom et al.*, 1978; *Arvidson et al.*, 1982, 1989]. Analysis of ISM and TES data has provided mineralogical interpretations of these regions and has allowed variations within them to be mapped [*Murchie et al.*, 1993, 2000; *Mustard and Sunshine*, 1995; *Bandfield et al.*, 2000b; *Bandfield*, 2002].

[8] ISM observations of dark gray regions reveal strong 1 and 2 μm absorptions due to ferrous iron in the surface materials in the form of pyroxene minerals [*Bibring et al.*, 1990]. The center of the absorption bands vary within and among the separate dark gray regions suggesting variations in the pyroxene compositions [*Mustard and Sunshine*, 1995; *Mustard et al.*, 1997]. Analysis of these absorptions using the Modified Gaussian Model show that low- and high-calcium pyroxenes are required for fitting the spectral reflectance, consistent with the lithologies of basaltic SNC samples [*Mustard and Sunshine*, 1995; *Mustard et al.*, 1997] as well as a range of intermediate to ultramafic lithologies. The NIR spectral slopes (decrease in reflectance with wavelength) are variable in dark gray regions as well. Syrtis Major in particular shows that the spectral slope varies from east to west and has been hypothesized as arising from coatings on the rocks in this region [*Mustard et al.*, 1993; *Murchie et al.*, 2000].

[9] Data from TES indicate two primary types of dark gray material typified by spectra from Syrtis Major (Type I) and Acidalia Planitia (Type II) [*Bandfield et al.*, 2000b]. Mineral spectra mixing models suggest their spectral differences arise from mineralogy, where Type I regions contain-

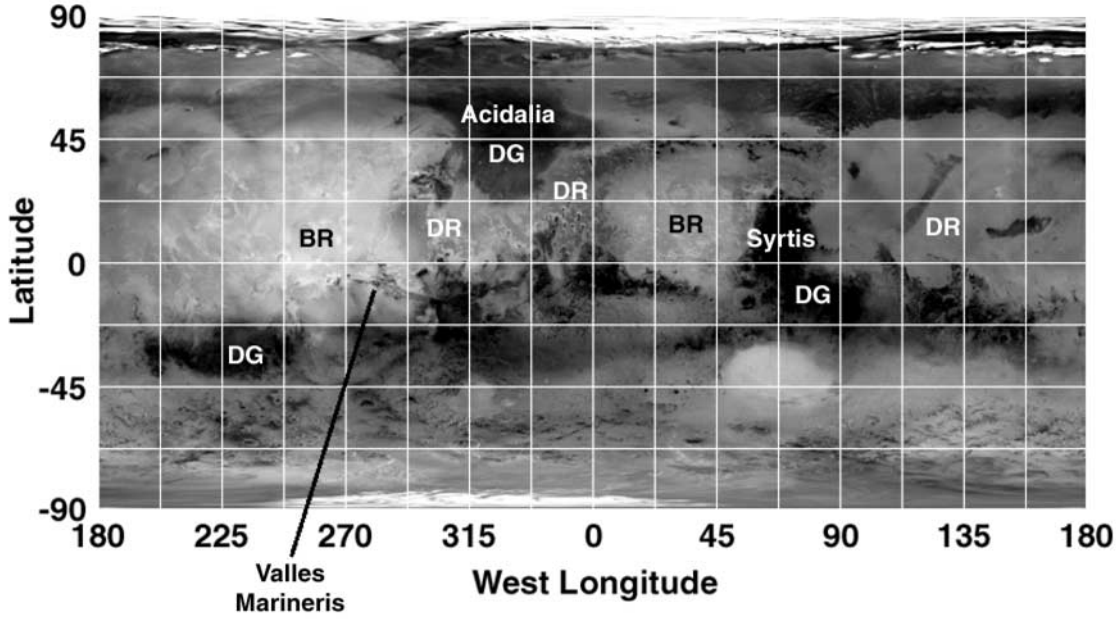

Figure 1. Viking albedo map with dark gray (DG), bright red (BR), and dark red (DR) major surface types labeled. Also shown are the locations of dark gray surfaces (Valles Marineris, Acidalia Planitia, and Syrtis Major) analyzed in this work.

ing materials that are more mafic (basaltic) and Type II regions containing more silicic materials (basaltic-andesite to andesite in composition) [*Bandfield et al.*, 2000b; *Hamilton et al.*, 2001]. Other proposals have been raised to explain the fundamental differences between the two spectral types including weathering and alteration processes [*Noble and Pieters*, 2001; *Wyatt and McSween*, 2002], oxidation state [*Minitti et al.*, 2002], water content [*Minitti et al.*, 2000], glass composition [*Noble and Pieters*, 2001], and degree of crystallinity [*Minitti et al.*, 2002].

[10] Clearly the separate wavelength regimes are providing information on the major component mineralogy (such as the coordination and oxidation states of iron and the types of silicates), but may be responding to different subtleties such as coatings, alteration, oxidation, and particle size. Issues that can be addressed by combining the data sets from these separate wavelength regions include determining the relationship between pyroxene absorptions and modeled mineral/rock compositions from deconvolution, discovering whether coatings or weathering may be altering spectra, and understanding the fundamental variations that exist among dark regions.

[11] Despite the wealth of knowledge represented by these observations from diverse regions of Mars, they have arisen primarily from separate analyses of individual data sets. A more detailed understanding can be obtained by investigating the interrelationships between spectra in the different wavelength ranges. Additionally, potential surface changes can be identified over the decadal timescales between the measurements of different instruments. There were very few apparent changes in surface reflectance between Viking and ISM observations of the surface of Mars [*Mustard et al.*, 1993]. However there has been an increase in the number of dust storms since 1990 [e.g., *Martin and Zurek*, 1993; *Malin et al.*, 1998] and thus here may have been changes in the surface reflectance between ISM and TES. Changes of albedo markings have been noted before and are often due to the redistribution of dust by winds [*Lee*, 1987].

3. Data Processing and Methods

[12] In order to carry out an analysis of the spectral properties of the surface of Mars across the extended wavelength range from visible to thermal infrared, the data sets from the individual instruments must be brought together.

[13] The reduction and calibration of ISM data have been reported on in detail previously and will not be repeated here [*Mustard et al.*, 1993; *Erard and Calvin*, 1997]. Briefly, all well characterized instrumental, solar, and atmospheric effects are removed in a series of additive and multiplicative steps. Absorptions due to H_2O, CO, and CO_2 are removed using an exponential function of wavelength-dependent absorptivity and atmospheric path length (elevation and viewing geometry). Scattering by aerosols and dust in the atmosphere is a function of atmospheric opacity and the ISM data were acquired during the period when atmospheric opacity was low [*Martin and Zurek*, 1993]. The spectral contribution of aerosols is dominated by a negative continuum slope which decreases exponentially toward a minimum near 2.6 μm, and the total relative contribution to the surface signal at shorter wavelengths is estimated to be 5–15%. This has been removed using the model of *Erard et al.* [1994]. Absolute radiometric accuracy is estimated to be 15% [*Erard et al.*, 1994], but the channel to channel precision is much higher (≈0.5%) which allows the identification of mineralogy and the mapping of subtle

spectroscopic features. The calibration of ISM has been validated against independent data sets in the visible-near infrared [*Mustard and Bell*, 1994] and short wavelength near-infrared [*Erard and Calvin*, 1997].

3.1. Data Selection and Processing of TES Data

[14] The processing steps for TES data involve selecting and correcting raw spectra, spatially aligning the data sets, transforming them into geologically useful measurements, and joining with ISM data into a single, coherent product. After the fusion has been accomplished, comparisons can be made between the two spectral regions and among the extended spectra of diverse geographic areas.

[15] TES data are collected with a Fourier-transform Michelson interferometer and have 5 or 10 cm^{-1} spectral sampling over the range of 1709–200 cm^{-1} (~6–50 μm). As the vast majority of the spectra are at 10 cm^{-1}, we have chosen to only work with these observations. Not all of the observations were of equal quality which necessitated subsetting the data and selecting only the best quality spectra. Many parameters control quality, and the relevant values are reported in the TES metadata, allowing for easy identification. The signal-to-noise ratio (SNR) depends on the surface temperature and we extracted observations above 260 K in order to maximize SNR. We also use observations with emission angles <20° to minimize atmospheric interference with the surface signals. Further project flags identify conditions (such as spacecraft or solar panel motion, etc.) that may result in lower quality data, and these flags were required to be at their highest level. A final screen was performed to eliminate any remaining spectra that contained obvious, large amounts of noise in the form of spikes or discontinuities. The result of screening the data is a collection of ~13.1 million high-quality radiance spectra.

[16] These spectra are converted into surface emissivity following the methods of *Christensen et al.* [1998], *Smith et al.* [2000], and *Bandfield et al.* [2000a]. First the spectra are transformed to brightness temperature spectra by inverting the Planck function to find the corresponding temperature for each radiance measurement. The three greatest brightness temperatures from the channels between 317–1333 cm^{-1} are then averaged to find the maximum brightness temperature. Because silicates typically have a Christiansen feature at 1050–1350 cm^{-1} (7–10 μm) [e.g., *Salisbury et al.*, 1991], where they are nearly perfect blackbodies (emissivity, $\varepsilon \approx 1$), the maximum brightness temperature can be assumed to be equal to the actual kinetic temperature of the surface material. Dividing the measured radiance spectrum by the spectral radiance for a blackbody with a temperature equal to the maximum brightness temperature therefore produces the apparent emissivity spectrum of the surface.

[17] This apparent emissivity spectrum contains both the spectral information from the surface and a contribution from the atmosphere through which the radiation passed. To separate these two signals, we have taken the approach presented by *Bandfield et al.* [2000a]. This method assumes that the surface and atmospheric signals mix linearly in emissivity space. Because the Martian atmosphere is thin, this approximation is valid when cloud cover and dust loading are low based on comparisons to independent techniques [*Bandfield et al.*, 2000a; *Smith et al.*, 2000]. Uncertainty and error may be introduced into the resultant emissivity spectra. Any residual misfit from the atmospheric portion of the model gets partitioned into the derived surface spectra. Any surface materials that spectrally resemble atmospheric components will be partitioned into the atmospheric components and not represented by the resultant surface spectra. A similar situation can arise when dealing with atmospheric components across transparent portions of the spectra, as surface spectral features in the transparent region may be mistakenly introduced into the atmospheric end-member.

3.2. Spectral Mixture Analysis

[18] Spectral Mixture Analysis (SMA) is used to find the relative abundances of the surface components and the atmospheric end-members. Once the atmospheric portions are identified, they are removed from the original spectral measurements to produce the surface emissivity spectra.

[19] The library of end-members used in the SMA is important. Four atmospheric components were derived by *Bandfield et al.* [2000b] using the target-transform technique and consist of two atmospheric dust and two water-ice cloud spectra (Figure 2). The surface materials used as end-members included the three surfaces described by *Bandfield et al.* [2000b]. In detail, these end-members include two igneous rock surface spectra from Syrtis Major (Type I) and Acidalia Planitia (Type II) from *Bandfield et al.* [2000b]. The third surface spectral end-member is from the coarse-grained specular hematite region in Sinus Meridiani that has been described by *Christensen et al.* [2000].

[20] SMA models each individual TES spectrum as a linear combination of the emissivity spectra of the end-member components and to separate the surface and atmospheric components. A blackbody (unity emissivity at all wavelengths) was included as a spectral end-member to adjust the contrast of the other end-members properly. The model results in a set of linear weights which represent the fractional abundance of each end-member material. As the model was performed, end-members with negative abundances were removed and the SMA was repeated iteratively until all end-member abundances were positive. This process has been used by other workers [*Ramsey and Christensen*, 1998; *Feely and Christensen*, 1999; *Bandfield et al.*, 2000b; *Hamilton and Christensen*, 2000] and forces the model to produce results that make sense physically, although it results in somewhat higher RMS errors.

[21] Atmosphere-removed emissivity spectra were produced for each TES measurement by subtracting the atmospheric end-members weighted by their model abundances and the portion of the blackbody related to the atmosphere from the measured spectra of Mars. The blackbody was partitioned so that the sum of the surface end-member abundances and the surface-related blackbody equaled one. This has the result of ensuring the continuum level for the emissivity spectra is near unity thereby giving the appropriate emissivity spectra for the Martian surface.

[22] The atmosphere-removed surface emissivity spectra were then averaged into a global data grid at a resolution of 0.25° per pixel. This grid provides for continuous coverage across most regions between 70° N and S latitude while

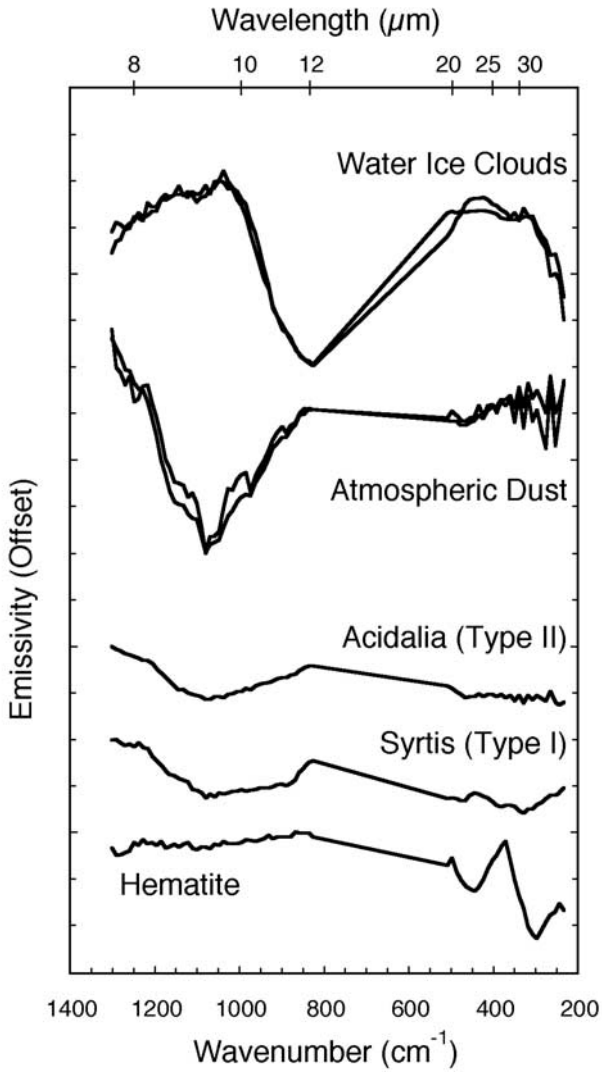

Figure 2. End-members used in the spectral mixture analysis of TES data. Spectra offset for clarity.

maximizing spatial resolution. The fractional abundances of the surface end-members were similarly gridded, as was the vis-NIR albedo from the bolometer, and statistics on the number of observations in each cell of these grids are shown in Figure 3a.

3.3. TES-ISM Data Fusion

[23] This final set of TES surface emissivity was then combined with the ISM visible to near-infrared reflectance data. Six of the ISM data cubes were sampled to the same 0.25° per pixel grid as the TES data. These data were coregistered using pointing information using a first order polynomial fit together with nearest neighbor resampling to preserve the actual spectra. Because the two instruments use slightly different coordinate systems, the data were then adjusted so that discrepancies along edges of high-contrast features such as Valles Marineris were minimized when comparing the TES visible albedo to the averaged ISM albedo. Before joining, the TES data were converted to a reflectance scale by subtracting the emissivity from one for easier comparison to the ISM data. A spatial comparison of the data are shown in Figure 3b, with examples of the joined spectra plotted in Figure 4.

3.4. Band Parameters

[24] The strengths of absorption bands in the ISM data were calculated according to the method of *Clark and Roush* [1984]:

$$BS = 1 - \frac{R_b}{R_c}, \tag{1}$$

where the continuum reflectance R_c was the average of the reflectance from wavelengths on the continuum on either side of the absorption band. The reflectance of the absorption band R_b was measured at the band center. Band strengths were measured for the 1 and 2 μm ferrous iron bands attributed to pyroxenes in the Martian surface material. The continuum points and band centers for these three bands are listed in Table 2 and were used from previous works [*Mustard et al.*, 1997; *Murchie et al.*, 2000]. Although the 1 μm ferrous iron band was calculated, it is primarily not used because it is difficult to separate from overlapping ferric iron absorptions using a simple band parameter [*Murchie et al.*, 2000].

[25] The spectral slope was also calculated for the ISM portion of the data. The slope was defined as the change in reflectance from the average of the three wavelength channels 2.44, 2.49, and 2.53 μm to the average of the two channels 1.68 and 1.73 μm divided by the wavelength difference (2.49–1.70 μm) for the range between the two averages [*Mustard et al.*, 1997; *Murchie et al.*, 2000]. The overall albedo for the vis-NIR region was calculated from

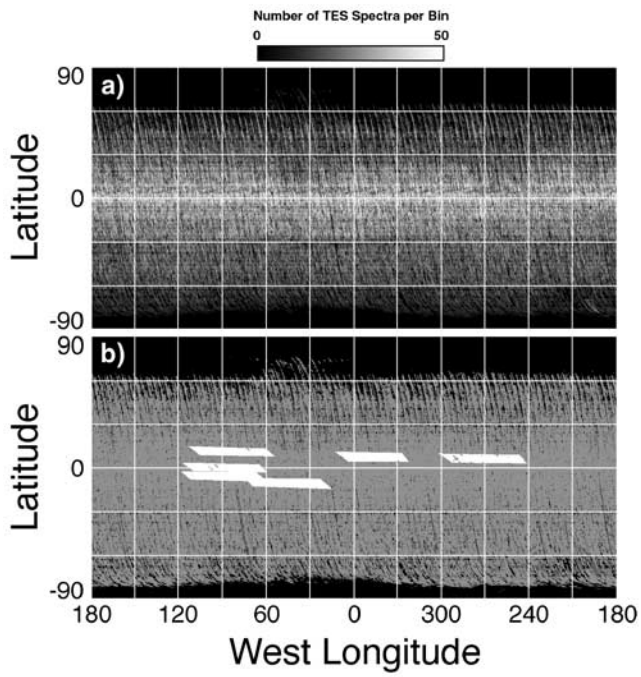

Figure 3. (a) Gray scale map of the number of TES spectra in each grid bin (0 = black, 100 = white). (b) Map showing the coverage of ISM (white) and TES (gray) spectra.

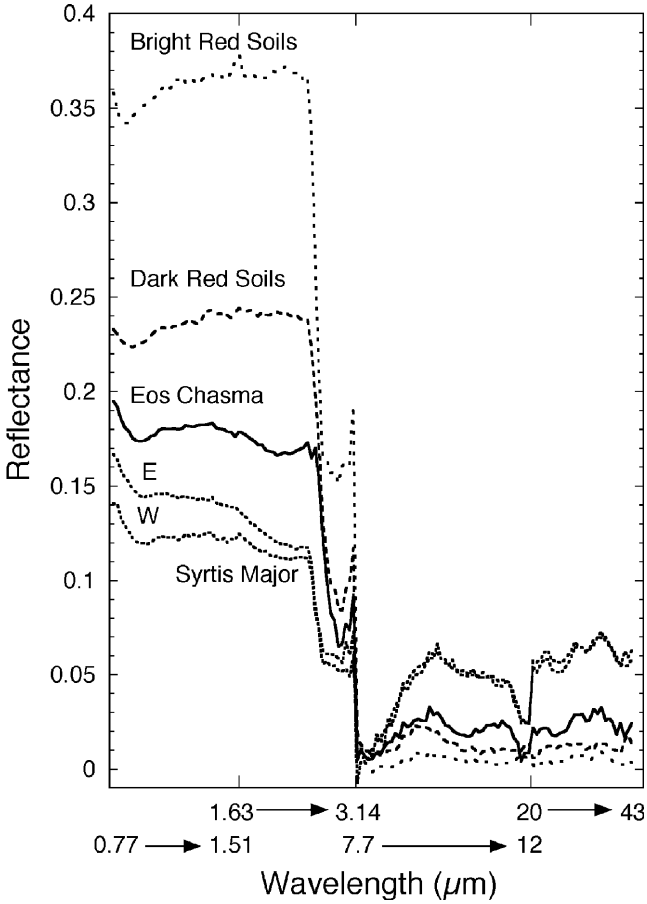

Figure 4. Examples of joined ISM-TES spectra from a variety of types of Mars surfaces covered by both instruments.

the ISM by averaging the spectral reflectances from each of the 32 channels from 0.77 to 1.51 μm. Albedo was also available from the TES visible bolometer which measured the albedo for the 0.3 to 2.7 μm range.

4. Results

[26] The analyses methods described above were applied to all of the ISM/TES joint data and resulted in a number of interesting observations, demonstrating the importance of working with spectral data from multiple wavelength regimes. Specific analytical methods varied in importance across geographic regions of Mars. The results are presented below by geographic region in order to emphasize how a better understanding of each region can be reached through the joint analysis approach.

4.1. Dark Gray Regions

[27] In general, low-albedo regions show a number of significant correlations between spectral behavior in the ISM and TES wavelength ranges. Because low-albedo regions are generally thought to consist of mafic rocks, the spectral characteristics in each wavelength region should reflect this. In the NIR, pyroxenes exhibit broad absorptions due to electronic absorptions in ferrous iron and are centered around approximately 1 and 2 μm. In the TIR, the absorptions are more complex and arise from the silicate structures not only of the mafic minerals (particularly pyroxene and olivine), but also feldspars. These compositions can be modeled either as surface end-members (such as Type I and II [*Bandfield et al.*, 2000b]) or a combination of minerals [*Bandfield et al.*, 2000b; *Hamilton et al.*, 2001; *Bandfield*, 2002; *Wyatt and McSween*, 2002].

[28] Comparing the results from the NIR band depth calculations with the TES surface unmixing and mineral deconvolutions shows strong correlations among these parameters for dark areas. Type I fractional abundance (the Syrtis or "basaltic" end-member) is relatively well correlated with the 2 μm band depth (Figure 5a) when measured across all dark regions. Zeroing in on the Syrtis Major region shows that the ISM band strengths and TES Type I abundances are even better correlated (Figure 5b), likely due to a more consistent regional composition in Syrtis Major compared to the complete data set. These results indicate that the surface abundance of mafic rocks mapped as Type I covary with the expression of pyroxene crystal field absorption, and that significant variations in pyroxene abundance are not indicated.

[29] The correspondence between Type II fractional abundance (the Acidalia or "andesitic" end-member) and the NIR pyroxene absorptions is weak (Figure 5c). However, the regions of Mars observed by ISM do not include Acidalia Planitia, the type region for Type II spectra. Only limited portions of Syrtis Major viewed by ISM have Type II fractional abundances up to 50%, making analysis of this end-member difficult. What data there are though show a weak correlation between Type II end-member abundance and vis-NIR band strengths even in this single scene (Figure 5d).

[30] Comparisons of the 1 and 2 μm band depths with the results from mineral deconvolutions of the TES spectra also highlight the signature of pyroxene. The correlation between spectroscopically derived mineral abundances in the TIR and the 2 μm band strength is shown for selected spectra from low-albedo regions (Figure 6). These spectra were taken from an east-west transect across Syrtis Major, as well as samples from Valles Marineris and Sinus Meridiani (away from the hematite zone). The 1 μm band behaves similarly but can include effects of other mafic and ferric minerals. The 2 μm band is correlated with pyroxene abundance (Figure 6a) and anticorrelated with blackbody amount (Figure 6b). However, the ratios of pyroxene abundance to either plagioclase abundance (Figure 6c) or total mineral abundance (Figure 6d) show much weaker relationships with the ISM band strengths. Finally, these TIR solutions typically find only a single, high-calcium pyroxene (although its identity may vary from spectrum to spectrum), in contrast with the findings of other workers that both low- and high-calcium pyroxenes were needed to model the 1 and

Table 2. Band Parameters

Band	Continuum	Band Center	Continuum
1 μm	0.81 μm	0.98 μm	1.36 μm
2 μm	1.68 μm	2.15 μm	2.49 μm
3 μm	2.49 μm	2.96, 3.00, 3.05 μm	

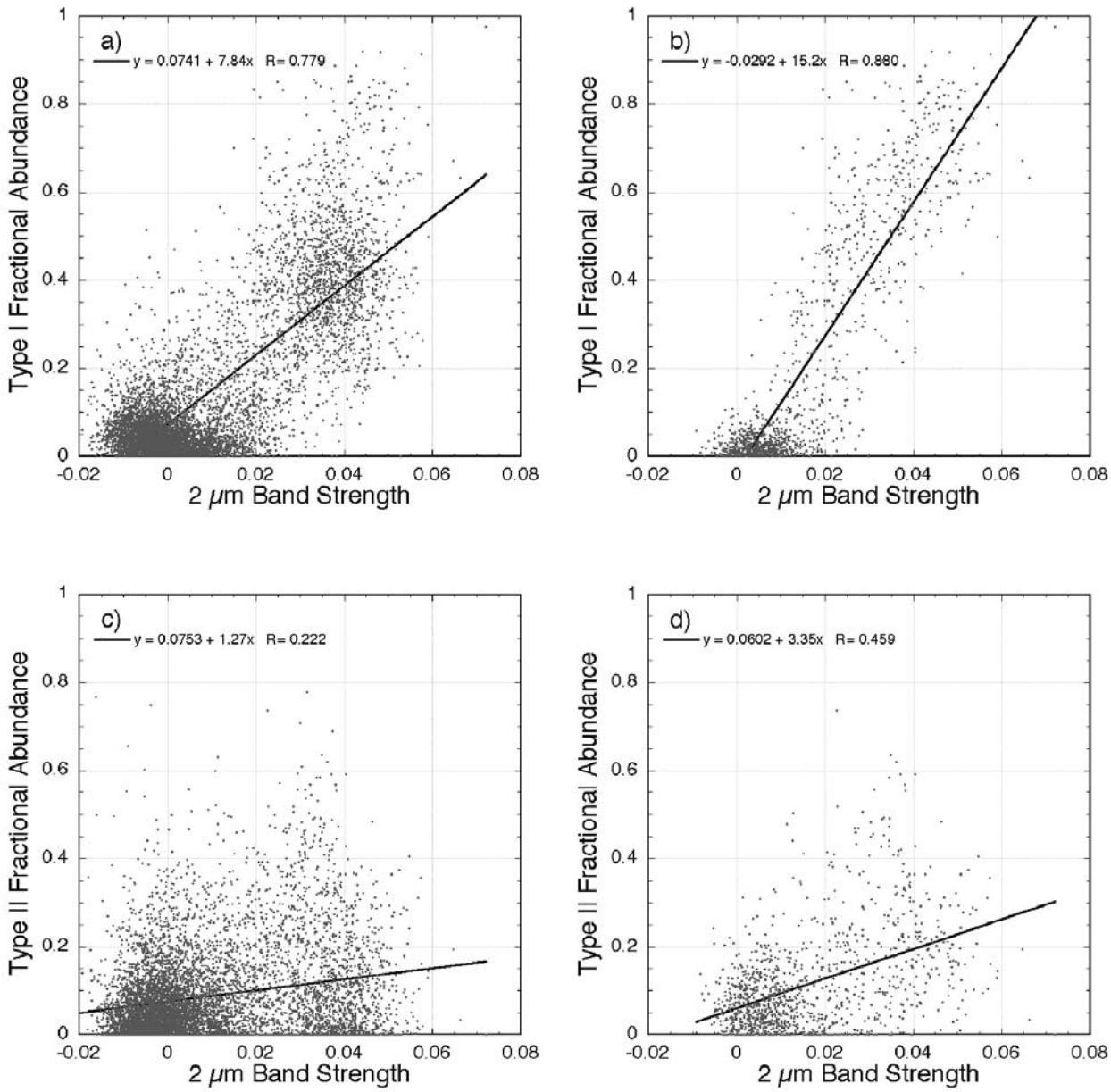

Figure 5. Scatterplots showing the relationships between 1 μm band depth and the following TES low-albedo end-members: (a) Type I for data from all ISM windows, (b) Type I for data from the Syrtis window only, (c) Type II for data from all ISM windows, and (d) Type II for data from the Syrtis window only.

2 μm bands [*Mustard and Sunshine*, 1995; *Mustard et al.*, 1997].

4.2. Syrtis Major

[31] Visual comparison of spectra from eastern and western Syrtis Major (Figure 7a) reveal strong differences in the slope in the vis-NIR region, as noted by previous workers [*Mustard et al.*, 1993; *Murchie et al.*, 2000]. In the western half, the vis-NIR has a relatively flat continuum, while eastern Syrtis Major has a strong negative slope. The differing behaviors in the two spectral regions can be quantified and are readily apparent from the average spectra of eastern and western Syrtis Major (Figure 7b). The average vis-NIR slope for eastern Syrtis is -0.014 ± 0.005, compared to an average of -0.023 ± 0.002 for western Syrtis. The standard deviation of the sampled spectra from the two portions of Syrtis Major are also shown in Figure 7b and demonstrate that the difference in spectral slope is significant. The spatial distribution of spectral slope in this region is shown in Figure 8a.

[32] In contrast there is little difference in the TIR spectra from the two sides of Syrtis Major. All of the spectra have

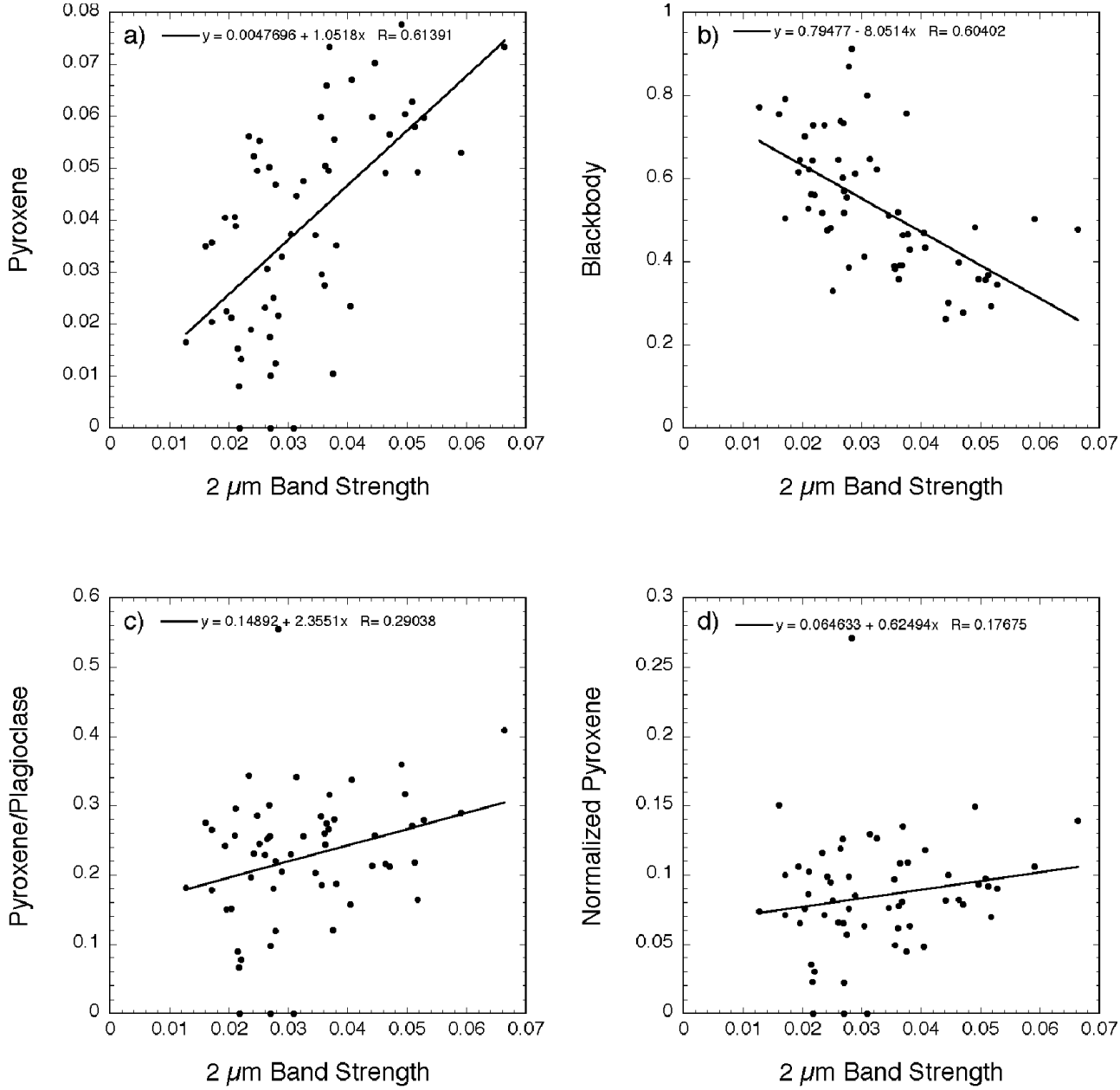

Figure 6. Scatterplots showing the relationships between 2 μm band depth and the results from mineral mixture modeling: (a) pyroxene abundance, (b) blackbody abundance, (c) pyroxene/plagioclase ratio, and (d) pyroxene abundance normalized by sum of all minerals.

the same shape in this wavelength regime (Figure 7a). Calculation of average spectra and standard deviations confirms the visual observations. The average TIR spectra for eastern and western Syrtis Major are very similar and fall within one standard deviation of each other (Figure 7b).

[33] As noted above, TES also measured vis-NIR albedo. Comparisons of the TES and ISM albedo (Figures 8b–8d) show that different albedo patterns are visible in the TES and ISM views of Syrtis Major. In the ISM view (Figure 8b), created from the average of individual reflectance channels, the western half is darker (0.11) than the eastern half (0.14). This contrasts with the TES map of albedo (Figure 8c), which shows that the western and eastern portions of Syrtis Major have approximately the same overall albedo (0.11–0.12). These differences do not appear to be related to simple calibration differences between the two instruments as the ratio of the two (Figure 8d) is strongly dependant on the geographic location.

[34] A comparison of all albedo measurements from the complete set of ISM windows and TES bolometer is shown in Figure 9. The two measurements are strongly correlated, as expected, but they are not equal and thus do not fall on a one-to-one slope. Instead, the best fit line shows that ISM and TES vis-NIR albedos are generally related by a multiplicative factor. TES albedos appear darker by a factor of ~0.79. The best fit line does pass through the origin, though, indicating that there is no offset between these two data sets. There are a number of differences in the

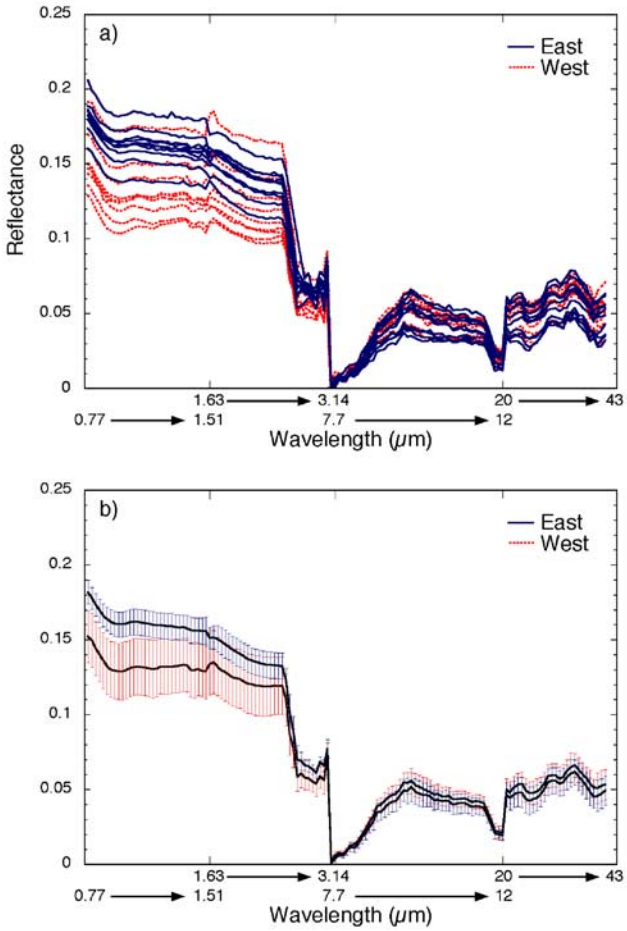

Figure 7. Comparison of joined ISM-TES spectra from eastern and western Syrtis Major. (a) Sample spectra from an E-W transect and (b) average spectra and standard deviations for eastern and western Syrtis Major.

measurement of albedo between the two instruments that may account for the multiplicative factor. First and most importantly, the wavelength regions are not the same (0.77–1.51 μm for ISM, 0.3–2.7 μm for TES), with ISM measuring multiple channels that are averaged together and TES measuring a single, broad channel. This means that TES picks up more of the ferric absorption in the UV-VIS, darkening the overall albedo relative to ISM. Also, the ISM measurements were obtained in a single day, while the TES albedo was built up over a period of months to years. Given these differences in methodology, it is unsurprising that the albedos do not fall on a one-to-one line, but the strong linear correlation with just a multiplicative offset shows the good overall agreement of the two data sets.

[35] All of the data does not cluster equally well along the best fit line, however. Some regions appear brighter in TES relative to the general trend. Mapping these regions of TES-ISM albedo misfit shows that one such area is in western Syrtis Major (Figure 8d), as noted above. In the western portion of Syrtis Major, the ratio of TES to ISM albedo is 1.15, while in the eastern half it is 0.85. In comparison, the rest of the region covered by this ISM window is relatively uniform in the albedo ratio of 0.78, similar to the trend of the global comparison (0.79). This shows that western Syrtis Major had a significant difference in albedo at the time of the TES measurements compared to the ISM measurements, while the eastern portion and surrounding areas including Isidis Planitia appear nearly unchanged.

5. Discussion

[36] The joint analysis of NIR and TIR spectral data sets for Mars reveals interesting consistencies and differences. The wavelength regimes represented by ISM and TES spectral data respond to different types of absorption processes: crystal field electronic transitions, charge transfer, and molecular vibrations in vis-NIR wavelength regions and lattice-mode vibrations for the TIR. In some cases these different pieces of information are complementary and provide confirmation and reinforcement of compositional identification. In other cases the information provided by the ISM and TES data give separate pieces of the compositional makeup which when taken together provide a clearer picture of the surface mineralogy and composition. Finally, some of the data is conflicting and raises additional

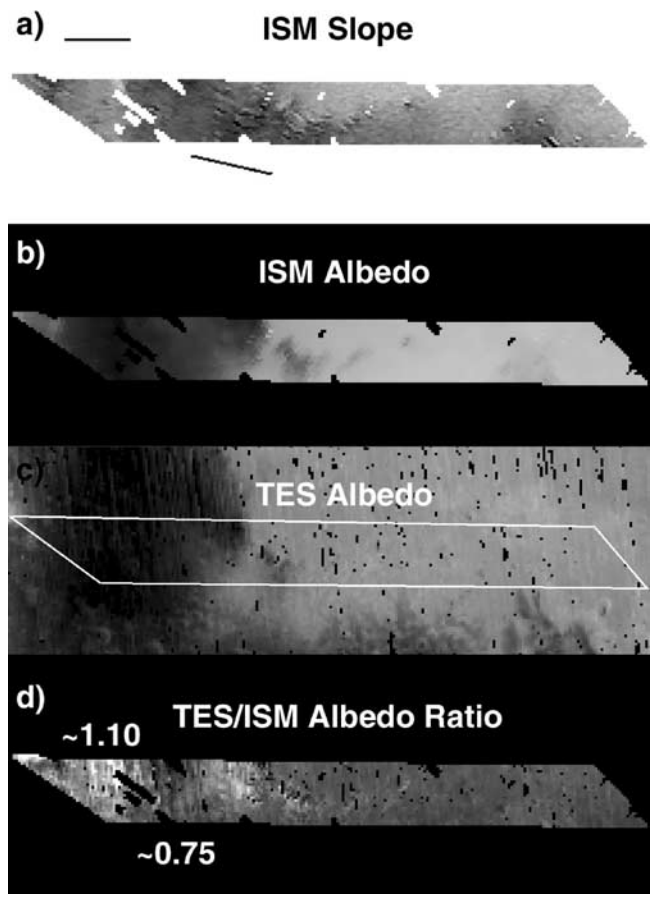

Figure 8. Maps of spectral parameters from the Syrtis Major region. (a) ISM vis-NIR slope (darker regions have steeper negative slopes), (b) ISM vis-NIR albedo, (c) TES vis-NIR albedo, and (d) ratio of TES and ISM albedos (lighter tones indicate areas that have brightened between the time of ISM and TES measurements).

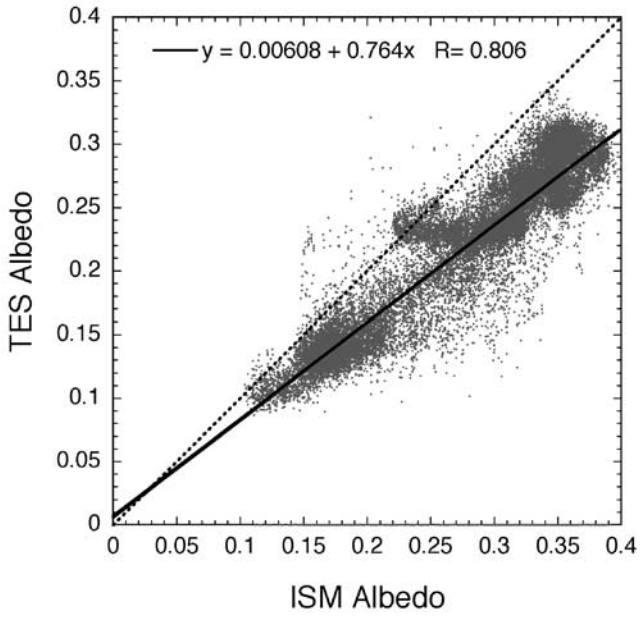

Figure 9. Scatterplot showing the relationship between ISM and TES measurements of vis-NIR albedo, together with best fit (solid) and one-to-one (dashed) lines.

questions about theories that had been based on observations from only one or the other of the wavelength regimes.

5.1. Composition of Dark Gray Regions

[37] Each wavelength range reinforces the conclusions drawn from the other. Both vis-NIR and TIR indicate the presence of pyroxene, although the type and even the number of pyroxenes present are not resolved. The correlations of the 1 and 2 μm band strengths with the abundance of Type I material and with the abundance of pyroxene from mineral mixing models show the pyroxene absorptions have a strong effect on the spectra in both wavelength regions. However the total absorption strength in the TIR, which controls the abundance of Type 1 material, has additional components such as feldspar that are not resolved in the vis-NIR.

[38] The joint analysis of the NIR and TIR yield more than just confirmation of mafic minerals however. The two sets of data provide insight into the nature of the variation in surface materials. The 1 and 2 μm band strengths are inversely correlated with blackbody abundances used in the SMA solutions, but they are not correlated in any way with the ratio of pyroxene to other minerals singly or as a whole. Because loose dust is spectrally bland, it resembles a simple blackbody and is represented strongly in this SMA model by the blackbody component. Taken together, the types of correlation between the pyroxene-caused 1 and 2 μm bands and the mineral mixing models indicate that variations in Type I dark gray regions are dominated by the mixing of loose dust and dark gray lithics (either rocks or sand-sized fragments). Variations in rock composition would have resulted in the correlation of the 1 and 2 μm pyroxene features with the relative abundance of pyroxene compared to other minerals, which was not observed.

[39] Conceptually this mixing line can be shown on a ternary diagram with vertices that represent pyroxene, dust, and other minerals (Figure 10). The 1 and 2 μm band strength would be constant for constant total abundances of pyroxene (horizontal lines in Figure 10). Variations in these band strengths can thus come by adding either of the other two components in the system. But since the pyroxene to other mineral ratio does not correlate with the pyroxene band strengths while the blackbody component does (inversely), the only mixing line in the system must be radial from the blackbody (dust) vertex. This implies a single composition for the rocks that mix with the dust, with the composition specified by the intercept of the mixing line on the pyroxene-other mineral edge of the diagram.

[40] An important difference between analyses of ISM and TES data in the Type I regions is the number and type of pyroxenes present in the dominant rock composition. Analyses of the vis-NIR bands using the Modified Gaussian Model show the need for two pyroxenes, one high-calcium and one low-calcium, to fit the shape of these absorption bands [*Mustard and Sunshine*, 1995; *Mustard et al.*, 1997]. However, mineral deconvolution of TES data from these same regions are different. Some results show only a single, high-calcium pyroxene is required with amounts >10% [*Bandfield et al.*, 2000b; *Hamilton et al.*, 2001], while others with alternate end-member libraries show both high- and low-calcium pyroxenes present at greater than 10% abundance [*Wyatt and McSween*, 2002]. Clearly more work needs to be done to resolve these differences. New vis-NIR observations by CRISM and OMEGA and the application of analysis methods to the full wavelength range (visible-thermal infrared) offer significant promise for complementary compositional and textural results.

[41] The situation with Type II regions is less clear. Because ISM did not sample the type locality for this

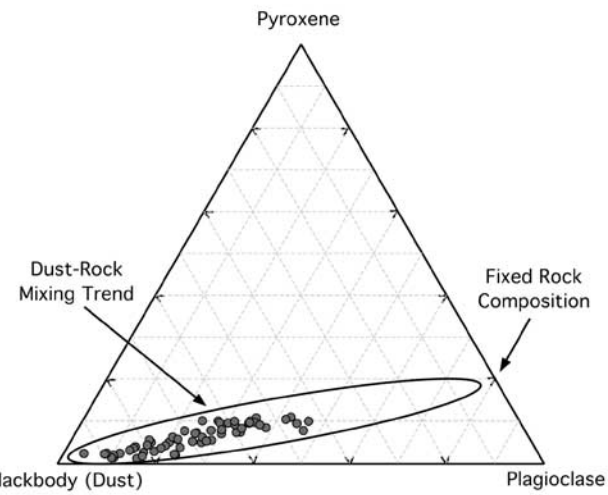

Figure 10. Ternary diagram illustrating the dust-rock mixing relationship in dark gray regions. Pyroxene to plagioclase ratio is fixed in this mixing trend, and variations in pyroxene abundance and 1 and 2 μm band strength are controlled by mixing of a fixed composition rock with a blackbody component, assumed to represent dust.

spectral end-member in Acidalia Planitia, our interpretations are limited to what can be learned from the portions of Syrtis Major that contain some Type II abundances. Small portions of Syrtis covered by ISM contain Type II abundances up to 50% which are only weakly correlated with 1 or 2 μm band strength (Figures 5c and 5d). The lack ISM observations over regions with high abundances of TES Type II material limit the degree of confidence regarding the presence or absence of any correlation with the vis-NIR pyroxene bands. If the lack of correlation were to be confirmed by future observations, it would suggest that Type II materials do not contain appreciable pyroxene. If these materials are mafic in nature, this could suggest that the pyroxenes in them have been weathered. Alternatively, they may not have contained pyroxene to begin with as with many lithologies of intermediate composition. Analyses of TES spectra of Type II materials suggest pyroxene contents of 10% [*Bandfield et al.*, 2000b] or 0% [*Hamilton et al.*, 2001], which raises two other possibilities. Either the surfaces in this part of Syrtis Major have been altered between ISM and TES observations, such as by the redistribution of dust by aeolian activity (see discussion below), or weathering in the form of penetrative oxidation [*Minitti et al.*, 2002] may have altered the ferrous iron in the near-surface regions of exposed pyroxene grains enough to affect their electronic spectra in the vis-NIR, but not change the silicate lattice enough to significantly affect the vibrational spectra in the TIR.

5.2. Variations in Surface Materials of Syrtis Major

[42] Previous analyses hypothesized the strong negative spectral slopes in the eastern half of Syrtis Major arise from the intimate mixture of sand-sized mafic grains and fine dust that has been bonded in place, possibly with a ferric cement or that that there are thin coatings on grains [*Mustard et al.*, 1993; *Murchie et al.*, 2000]. The western half of Syrtis Major is interpreted as having fresher grain surfaces with little to no dust. This portion of Syrtis Major is known to wax and wane in albedo as a function of dust deposition by winds [*Lee*, 1987], and when dust is mixed in, the spectra probably look more like other "transitional" dark regions that are interpreted as having simple checkerboard mixing of dust and dark mafic materials [*Murchie et al.*, 2000].

[43] If this theory of intimate mixing of dust and mafic materials is correct, then similar variations in the TIR spectrum should be seen. *Johnson et al.* [2002] have shown that thin coatings of fine particulate materials which behave as intimate mixtures give rise to rapid changes in spectral properties, not only in the vis-NIR, but also in the TIR. Therefore the fact that the TIR properties of eastern and western Syrtis Major are very similar implies that the intimate mixing theory is not valid and another hypothesis is needed.

[44] One possibility is that some other process has modified the material in one half of Syrtis Major in such a way that only the vis-NIR portion of the spectrum is affected. *Minitti et al.* [2002], using laboratory measurements of the spectral properties of basaltic-composition glasses, showed strong changes in the vis-NIR slope as oxidation state changed, but relatively little change in the TIR spectra. TEM analyses showed that oxidation was causing ultra-fine blebs of oxidized iron to form in the outermost layers of glass with these particles primarily less than 25 nm in diameter. This type of penetrative oxidation may be expected to cause changes in the vis-NIR regions where electronic transitions and charge transfers are very sensitive to the oxidation state of the iron. However, the particles are smaller than the wavelength of thermal infrared radiation and therefore do not act as coherent emitters, thus masking the molecular vibrational signature of these oxides in the same way that very fine particulates lack spectral contrast [*Lyon*, 1965; *Hunt and Vincent*, 1968; *Pieters*, 1983; *Crown and Pieters*, 1987; *Moersch and Christensen*, 1995; *Ramsey and Christensen*, 1998; *Cooper and Mustard*, 1999]. Furthermore, the penetrative oxidation in early stages would not alter the pyroxene and feldspar structures, which would allow these minerals to still dominate the TIR spectra and look very similar to their unoxidized counterparts.

[45] For this theory to be true, though, it requires that the vis-NIR and TIR information are taken from surfaces of the same composition and state. Variations in the vis-NIR albedo measured by the two instruments indicates that changes in albedo may have occurred. The western half of Syrtis Major appears to have lightened relative to the eastern half and the surrounding areas between the time of ISM (1989) and TES (1998–2001). This suggests that additional dust may have been deposited in these western regions during that timeframe, consistent with Viking era observations and the interpretations of eastern Syrtis Major being a dust source/sink over cycles of dust storms [*Lee*, 1987]. The albedo differences between the eastern and western halves that were observed along with the slope variations (Figure 8) may have been erased due to this redistribution of dust. Such changes could have occurred during the dust storm of 1998 that occurred soon after MGS reached Mars. If the two halves of Syrtis Major were truly homogenized, then no difference in the thermal infrared spectra would be expected, and the disagreement between the vis-NIR and TIR might be an artificial byproduct of comparing data taken at different times. If this is the case, differential mixing of dust at the time of the ISM observations could still be the driver for variations in vis-NIR slope in this dark gray region.

[46] However, the dust appears to have been added mostly to the western half and not the eastern half where the unusual vis-NIR slopes are observed. *Murchie et al.* [2000] hypothesized that if dust were deposited in western Syrtis Major that this area would look like transitional dark areas and not like the eastern half of Syrtis Major and would still not have the same slope properties as the eastern regions. This is due to the differences in the type of dust mixing, with normal checkerboard mixing that waxes and wanes predicted for western Syrtis and an intimate cementing of dust and mafic particles in eastern Syrtis. In this case the similarity of the thermal spectra form eastern and western Syrtis Major does indicate that the intimately bonded dust-mafic mixture that has been hypothesized is flawed and that penetrative oxidation may be the answer.

[47] In any event, these two theories explaining slope differences in Syrtis Major can be tested through further comparison of vis-NIR and TIR data taken more closely together in time. OMEGA and CRISM data will show whether the slope variations observed by ISM still exist.

If so, then the coating model is unlikely to be correct and penetrative oxidation may be an important phenomenon modifying the surface of Mars. On the other hand, if OMEGA and CRISM show little variation in spectral slopes in Syrtis Major, the redistribution of thin coatings of dust is the probable control on spectral properties in the vis-NIR.

6. Conclusions

[48] The joint analysis of ISM and TES spectral data has shown the benefits of working with a broader range of remote sensing information when tackling questions of surface compositions for Mars. Even though the two data sets were obtained over a decade apart and overlapped in only limited spatial regions, a number of important observations have been made. Some of these observations are complementary with each other, while others show differences in the two wavelength regions that in some cases suggest new interpretations of the surface composition.

[49] In the dark gray regions of Mars, the ISM and TES data agree quite well. Both point toward mafic compositions with pyroxenes as an important component of the surface materials. Type I end-member regions are dominated by pyroxene-bearing lithic material that mixes with bright red dust. The pyroxene may have either one or two compositions as the two spectral regions appear to disagree. Future observations in the vis-NIR at higher spatial resolutions and with greater coverage may help to resolve this issue. The limited observations by ISM of Type II areas suggest this end-member does not contain appreciable pyroxene, bringing into question the interpretation of this material as andesitic or basaltic-andesitic in composition. Instead, the lack of correlation between Type II abundance and 1 and 2 μm band strength is more consistent with weathered basalts where the pyroxenes have had surface oxidation that has affected the ferrous iron crystal field absorptions more than the silicate vibrational bands. However, changes were seen between ISM and TES in Syrtis Major where ISM overlapped with relatively high Type II concentrations, which may mean that changes in dust mixing are instead driving the lack of correlation between the vis-NIR and TIR data. Also, ISM did not observe the regions of greatest Type II abundance (Acidalia Planitia), and future observations of the rest of the globe in the vis-NIR may provide more insight.

[50] In Syrtis Major, the two portions of the joint spectra do not agree. Differences similar to the changes in NIR spectral slope from east to west are not apparent in the TIR. The relative difference in albedo between eastern and western Syrtis Major also appears to have changed over the course of the decade between ISM and TES measurements. These changes are likely due to redistribution of dust in the region. The cause of the slope differences are therefore uncertain, but can be tested by future missions. If the vis-NIR characteristics have changed and now have no slope differences from east to west, mirroring the TES data, then the cause of the original ISM slope variations is the mixing of fine layers of dust over the rock. The previously hypothesized coatings would not be as durable as once thought. If however the slope variations are still present, then a different process that affects the vis-NIR and not the TIR must be active. This rules out thin coatings and dust mixing, as both of these affect the TIR in a similar manner as the vis-NIR [*Johnson et al.*, 2002]. Instead a likely hypothesis is that penetrative oxidation is occurring and affecting the oxidation state of a fine layer of iron near the surface of grains but not rearranging the crystal lattice, much like was seen in laboratory experiments by *Minitti et al.* [2002].

[51] By examining only the small areas covered by ISM at 22 km resolution with both vis-NIR and TIR wavelengths, each of the above regions is better described than by simply using a single wavelength regime or by trying to just compare results without merging the data. The merging allows the recognition of the interplay of different electromagnetic phenomena and can lead to new hypotheses that analysis of only one portion of the data misses. This gives promise for future observations of the globe in vis-NIR wavelengths by the CRISM and OMEGA instruments. Many discoveries can be made with these data alone, as was the case with TES data, but more understanding will be gained by merging the data sets together. Questions about coatings and the composition of Type II regions will be particularly amenable to these studies as this work has shown, and other new insights will doubtless be achieved.

[52] **Acknowledgments.** Thanks are extended to Phil Christensen, Vicky Hamilton, and Steve Ruff for assistance in understanding and processing TES data. Janice Bishop and Josh Bandfield provided thoughtful reviews that helped strengthen the findings. This work was supported by the Mars Data Analysis Program.

References

Arvidson, R. E., E. A. Guinness, and A. P. Zent (1982), Classification of surface units in the equatorial region of Mars based on Viking Orbiter color, albedo, and thermal data, *J. Geophys. Res.*, *87*, 10,149–10,157.

Arvidson, R. E., E. A. Guinness, M. A. Dale-Bannister, J. Adams, M. Smith, P. R. Christensen, and R. B. Singer (1989), Nature and distribution of surficial deposits in Chryse Planitia and vicinity, *Mars, J. Geophys. Res.*, *94*, 1573–1587.

Bandfield, J. L. (2002), Global mineral distributions on Mars, *J. Geophys. Res.*, *107*(E6), 5042, doi:10.1029/2001JE001510.

Bandfield, J. L., P. R. Christensen, and M. D. Smith (2000a), Spectral data set factor analysis and end-member recovery: Application to analysis of Martian atmospheric particulates, *J. Geophys. Res.*, *105*, 9573–9587.

Bandfield, J. L., V. E. Hamilton, and P. R. Christensen (2000b), A global view of Martian surface compositions from MGS-TES, *Science*, *287*, 1626–1630.

Bell, J. F., M. J. Wolff, P. B. James, R. T. Clancy, S. W. Lee, and L. J. Martin (1997), Mars surface mineralogy from Hubble Space Telescope imaging during 1994–1995: Observations, calibration, and initial results, *J. Geophys. Res.*, *102*, 9109–9123.

Bibring, J.-P., et al. (1990), ISM observations of Mars and Phobos: First results, *Proc. Lunar Planet. Sci. Conf. 20th*, 461–471.

Bibring, J.-P., et al. (2004), OMEGA: Observatoire pour la Minéralogie, l'Eau, les Glaces et l'Activité, *Eur. Space Agency Spec. Publ.*, *ESA-SP 1240*, 37–50.

Bibring, J.-P., et al. (2005), Mars surface diversity as revealed by the OMEGA/Mars Express, *Science*, *307*, 1576–1581.

Bishop, J. L., J. F. Mustard, C. M. Pieters, and T. Hiroi (1998a), Recognition of minor constituents in reflectance spectra of Allan Hills 84,001 chips and the importance for remote sensing on Mars, *Meteorit. Planet. Sci.*, *33*, 693–698.

Bishop, J. L., C. M. Pieters, T. Hiroi, and J. F. Mustard (1998b), Spectroscopic analysis of Martian meteorite Allan Hills 84001 powder and applications for spectral identification of minerals and other soil components on Mars, *Meteorit. Planet. Sci.*, *33*, 699–707.

Blaney, D. L., and T. B. McCord (1995), Indications of sulfate minerals in the Martian soil from Earth-based spectroscopy, *J. Geophys. Res.*, *100*, 14,433–14,441.

Burns, R. G. (1993), Origin of electronic spectra of minerals in the visible to near-infrared region, in *Remote Geochemical Analysis: Elemental and Mineralogical Composition*, edited by C. M. Pieters and P. A. J. Englert, pp. 3–29, Cambridge Univ. Press, New York.

Christensen, P. R., et al. (1998), Results from the Mars Global Surveyor Thermal Emission Spectrometer, *Science*, *279*, 1692–1698.
Christensen, P. R., et al. (2000), Detection of crystalline hematite mineralization on Mars by the Thermal Emission Spectrometer: Evidence for near-surface water, *J. Geophys. Res.*, *105*, 9623–9642.
Christensen, P. R., et al. (2001), Mars Global Surveyor Thermal Emission Spectrometer experiment: Investigation description and surface science results, *J. Geophys. Res.*, *106*, 23,823–23,871.
Christensen, P. R., et al. (2003), Morphology and composition of the surface of Mars: Mars Odyssey THEMIS results, *Science*, *300*, 2056–2061.
Clark, R. N., and T. L. Roush (1984), Reflectance spectroscopy: Quantitative analysis techniques for remote sensing applications, *J. Geophys. Res.*, *89*, 6329–6340.
Clark, R. N., G. A. Swayze, R. B. Singer, and J. Pollack (1990), High-resolution reflectance spectroscopy of Mars in the 2.3 μm region: Evidence for the mineral scapolite, *J. Geophys. Res.*, *95*, 14,463–14,480.
Conrath, B., R. Curran, R. Hanel, V. Kunda, W. Maguire, J. Pearl, J. Pirraglia, J. Welker, and T. Burke (1973), Atmospheric and surface properties of Mars obtained by infrared spectroscopy on Mariner 9, *J. Geophys. Res.*, *78*, 4267–4278.
Cooper, C. D., and J. F. Mustard (1999), Effects of very fine particle size on reflectance spectra of smectite and palagonitic soil, *Icarus*, *142*, 557–570.
Crown, D. A., and C. M. Pieters (1987), Spectral properties of plagioclase and pyroxene mixtures and the interpretation of lunar soil spectra, *Icarus*, *72*, 492–506.
Erard, S., and W. Calvin (1997), New composite spectra of Mars, 0.4–5.7 μm, *Icarus*, *130*, 449–460.
Erard, S., J.-P. Bibring, J. Mustard, O. Forni, J. Head, S. Hurtrez, Y. Langevin, C. Pieters, J. Rosenqvist, and C. Sotin (1991), Spatial variations in composition of the Valles Marineris and Isidis Planitia regions of Mars derived for ISM spectra, *Proc. Lunar Planet. Sci. Conf. 11th*, 437–455.
Erard, S., J. Mustard, S. Murchie, and J.-P. Bibring (1994), Martian aerosols: Near-infrared spectral properties and effects on the observation of the surface, *Icarus*, *111*, 317–337.
Feely, K. C., and P. R. Christensen (1999), Quantitative compositional analysis using thermal emission spectroscopy: Application to igneous and metamorphic rocks, *J. Geophys. Res.*, *104*, 24,195–24,210.
Gaffey, M. J., L. A. McFadden, D. Nash, and C. M. Pieters (1993), Ultraviolet, visible, and near-infrared spectroscopy: Laboratory spectra of geologic materials, in *Remote Geochemical Analysis: Elemental and Mineralogical Composition*, edited by C. M. Pieters and P. J. Englert, pp. 43–78, Cambridge Univ. Press, New York.
Hamilton, V. E., and P. R. Christensen (2000), Determining the modal mineralogy of mafic and ultramafic igneous rocks using thermal emission spectroscopy, *J. Geophys. Res.*, *105*(E4), 9717–9733.
Hamilton, V. E., M. B. Wyatt, J. H. Y. McSween, and P. R. Christensen (2001), Analysis of terrestrial and Martian volcanic compositions using thermal emission spectroscopy: 2. Application to Martian surface spectra from the Mars Global Surveyor Thermal Emission Spectrometer, *J. Geophys. Res.*, *106*, 14,733–14,746.
Hanel, R. A., et al. (1972), Investigation of the Martian environment by infrared spectroscopy on Mariner 9, *Icarus*, *17*, 423–442.
Hunt, G. R., and R. K. Vincent (1968), The behavior of spectral features in the infrared emission from particulate surfaces of various grain sizes, *J. Geophys. Res.*, *73*, 6039–6046.
Johnson, J. R., P. R. Christensen, and P. G. Lucey (2002), Dust coatings on basaltic rocks and implications for thermal infrared spectroscopy of Mars, *J. Geophys. Res.*, *107*(E6), 5035, doi:10.1029/2000JE001405.
Lee, S. W. (1987), Regional sources and sinks of dust on Mars: Viking observations of Cerberus, Solis Planum, and Syrtis Major, in *MECA Symposium on Mars: Evolution of Its Climate and Atmosphere*, edited by V. Baker et al., *LPI Tech. Rep. 87-01*, pp. 71–72, Lunar and Planet. Inst., Houston, Tex.
Lyon, R. J. P. (1965), Analysis of rocks by spectral infrared emission (8 to 25 microns), *Econ. Geol.*, *60*, 717–736.
Malin, M. C., et al. (1998), Early views of the Martian surface form the Mars Orbiter Camera of Mars Global Surveyor, *Science*, *279*, 1681–1685.
Martin, L. J., and R. W. Zurek (1993), An analysis of the history of dust activity on Mars, *J. Geophys. Res.*, *98*, 3221–3246.
Minitti, M. E., M. J. Rutherford, and J. F. Mustard (2000), The effects of oxidation on spectra of SNC-like basalts: Applications to Mars remote sensing, *Lunar Planet. Sci.*, *XXXI*, abstract 1282.
Minitti, M. E., J. F. Mustard, and M. J. Rutherford (2002), Effects of glass content and oxidation on the spectra of SNC-like basalts: Applications to Mars remote sensing, *J. Geophys. Res.*, *107*(E5), 5030, doi:10.1029/2001JE001518.
Moersch, J. E., and P. R. Christensen (1995), Thermal emission from particulate surfaces: A comparison of scattering models with measured spectra, *J. Geophys. Res.*, *100*, 7465–7477.
Murchie, S., J. F. Mustard, S. Erard, J. L. Bishop, J. W. Head, and C. M. Pieters (1993), Spatial variation in the spectral properties of bright regions on Mars, *Icarus*, *105*, 454–468.
Murchie, S., L. Kirkland, S. Erard, J. Mustard, and M. Robinson (2000), Near-infrared spectral variations of Martian surface materials from ISM imaging spectrometer data, *Icarus*, *147*, 444–471.
Murchie, S., et al. (2003), CRISM: Compact Reconnaissance Imaging Spectrometer for Mars on the Mars Reconnaissance Orbiter, in *Sixth International Conference on Mars*, abstract 3062, Lunar and Planet. Inst., Houston, Tex.
Mustard, J. F., and J. F. Bell III (1994), New composite reflectance spectra of Mars from 0.4 to 3.14 μm, *Geophys. Res. Lett.*, *21*, 353–356.
Mustard, J. F., and J. M. Sunshine (1995), Seeing through the dust: Martian crustal heterogeneity and links to the SNC meteorites, *Science*, *267*, 1623–1626.
Mustard, J. F., S. Erard, J.-P. Bibring, J. W. Head, S. Hurtrez, Y. Langevin, C. M. Pieters, and C. J. Sotin (1993), The surface of Syrtis Major: Composition of the volcanic substrate and mixing with altered dust and soil, *J. Geophys. Res.*, *98*, 3387–3400.
Mustard, J. F., S. Murchie, S. Erard, and J. Sunshine (1997), In situ compositions of Martian volcanics: Implications for the mantle, *J. Geophys. Res.*, *102*(E11), 25,605–25,615.
Noble, S. K., and C. M. Pieters (2001), Type II terrain: Compositional constraints on the Martian lowlands, *Lunar Planet. Sci.*, *XXXII*, abstract 1230.
Pieters, C. M. (1983), Strength of mineral absorption features in the transmitted component of near-infrared reflected light: First results from RELAB, *J. Geophys. Res.*, *88*, 9534–9544.
Pollack, J. B., T. Roush, F. Witteborn, J. Bregman, D. Wooden, C. Stoker, O. B. Toon, D. Rank, B. Dalton, and R. Freedman (1990), Thermal emission spectra of Mars (5.4–10.5 μm): Evidence for sulfates, carbonates, and hydrates, *J. Geophys. Res.*, *95*, 14,595–14,627.
Ramsey, M. S., and P. R. Christensen (1998), Mineral abundance determination: Quantitative deconvolution of thermal emission spectra, *J. Geophys. Res.*, *103*, 577–596.
Salisbury, J. W., L. S. Walter, N. Vergo, and D. M. D'Aria (1991), *Infrared (2.1–25 μm) Spectra of Minerals*, Johns Hopkins Univ. Press, Baltimore, Md.
Singer, R. B. (1982), Spectral evidence for the mineralogy of high albedo soils and dust on Mars, *J. Geophys. Res.*, *87*, 10,159–10,168.
Singer, R. B. (1985), Spectroscopic observations of Mars, *Adv. Space Res.*, *5*, 59–68.
Smith, M. D., J. L. Bandfield, and P. R. Christensen (2000), Separation of atmospheric and surface spectral features in Mars Global Surveyor Thermal Emission Spectrometer (TES) spectra, *J. Geophys. Res.*, *105*, 9589–9607.
Soderblom, L. A., K. Edwards, E. M. Eliason, and M. P. Charette (1978), Global color variations of the Martian surface, *Icarus*, *34*, 446–464.
Wyatt, M. B., and H. Y. McSween Jr. (2002), Spectral evidence for weathered basalt as an alternative to andesite in the northern lowlands of Mars, *Nature*, *417*, 263–266.

C. D. Cooper and J. F. Mustard, Department of Geological Sciences, Brown University, Box 1846, Providence, RI 02912, USA. (john_mustard@brown.edu)